MINI-RF OBSERVATIONS OF THE RADAR SCATTERING PROPERTIES OF YOUNG LUNAR CRATER EJECTA BLANKETS. G. W. Patterson[1], A. M. Stickle[1], D. B. J. Bussey[1], J. T. S. Cahill[1] and the Mini-RF Team, [1]Johns Hopkins University Applied Physics Laboratory, Laurel, MD (angela.stickle@jhuapl.edu).

Introduction: Impact cratering is a primary weathering process of airless bodies and is the dominant method of redistributing material across the lunar surface [1]. Crater ejecta blankets are a window into the impact cratering process and can provide important information regarding the properties of subsurface materials. Here, we use radar scattering information, in particular the circular polarization ratio (CPR) [e.g., 2] and an *m-χ* decomposition [3], to investigate properties of lunar crater ejecta. Previous work has examined the implications of radar scattering associated with the ejecta blanket of the crater Byrgius A for understanding ejecta thickness and emplacement mechanism [4]. We explore these and other potential contributions to the radar scattering properties of ejecta blankets for 23 additional craters distributed across the surface of the Moon and located in both mare and highland terrains.

Mini-RF background: The Miniature Radio Frequency (Mini-RF) instrument flown on NASA's Lunar Reconnaissance Orbiter (LRO) is a Synthetic Aperture Radar (SAR) with a hybrid dual-polarimetric architecture. I.e., the instrument transmits a circularly polarized signal and recives orthogonal horizontal and vertical linear polarizations (and their relative phase) [3]. The information returned by the radar can be represented using the classical Stokes parameters [S_1, S_2, S_2, S_4] [5], which can also be used to derive a variety of other products that are useful for characterizing radar scattering properties of the lunar surface.

To investigate the scattering properties of lunar crater ejecta blankets, we use two products derived from the Stokes parameters: the circular polarization ratio (CPR) and the *m-χ* decomposition of S_1. CPR information is commonly used in analyses of planetary radar data [e.g., 2,6], and is a representation of surface roughness at the wavelength scale of the radar (i.e., surfaces that are smoother at the wavelength scale will have lower CPR values and surfaces that are rougher will have higher CPR values). The *m-χ* decomposition provides information about the scattering characteristics of the surface (i.e., how much of the power returned is polarized and what is its polarization state) [3,7].

Methods: We have examined the radar scattering properties of ejecta blankets associated with 24 young, fresh, lunar craters with diameters ranging from 7-55 km. Average profiles of the Stokes parameters (e.g., S_1 and S_4), CPR, and the *m-χ* decomposition of S_1 were calculated as a function of radius for each crater. Profiles extend from the crater rim out to 7-10 crater radii (Fig. 2,3). For some of the craters, radial profiles were taken as an average over a select azimuthal range. This is especially useful for examining asymmetries in ejecta blankets due to oblique impacts or anomalous signals due to topography. The lunar crater Louville D serves as an example. Louville D is a 7-km crater on the western edge of Sinus Roris. This crater does not have an exceptionally bright ejecta blanket in optical images, but it shows up clearly in Mini-RF radar products (Fig. 1). A radially averaged profile that includes all azimuths shows a distinct spike in the S_1 parameter for Louville D. By excluding a specific azimuthal range from the profile, the source of the spike in S_1 can be isolated and, in this case, attributed to topography to the SW of the crater.

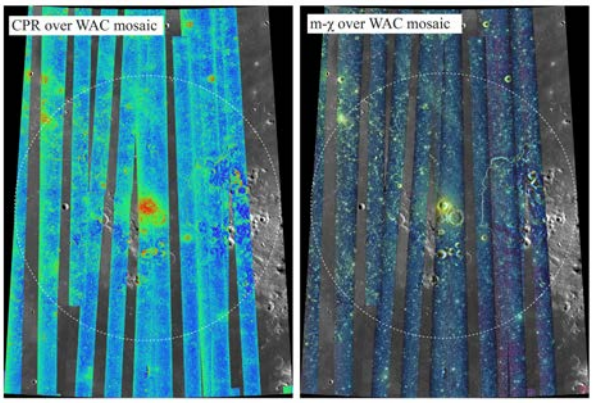

Fig. 1. Mosaics of the crater Louville D. Images show mosaics of Mini-RF data products overlain on the LROC WAC mosaic. Each image is 10°x10°, centered on the crater. The white dotted line indicates the edge of the profiles in Figure 2.

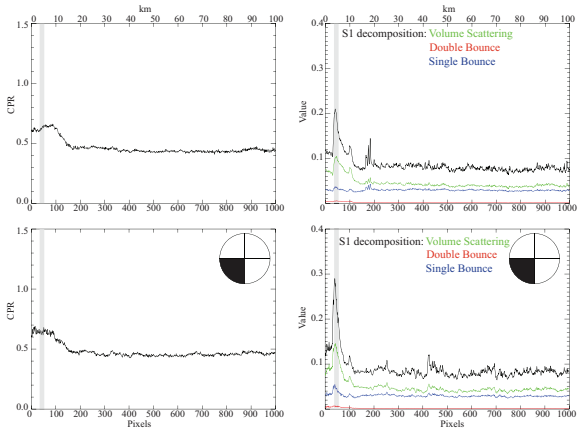

Fig. 2. CPR (left) and *m-χ* decomposition of S_1 (right) for the crater Louville D. (top) Profiles that include all azimuths, (bottom) profiles averaged over the SW quadrant of the ejecta blanket. The gray box shows the approximate extent of the "continuous" ejecta as visually identified by increased CPR signal.

Analysis: The twenty-four analyzed craters are spatially distributed across the lunar surface and in both mare and highland terrains. Though some commonalities in the scattering profiles are seen for all observed craters, differences are noted with crater diameter and between craters in different terrains. With the exception of a few select cases, mare craters exhibit lower CPR than those in the highlands. The absolute magnitude of CPR values between craters in the mare is also more uniform than in the highlands. Where present, regions of highest CPR near the crater rim (e.g., the red region in Fig. 1) tend to extend outward to ~0.5-1 crater radii, which is broadly consistent with estimates of continuous ejecta blanket deposition [1,8]. Beyond this region, the magnitude of the CPR for such profiles tends to transition to general lunar background levels (for example, Fig. 3A, beyond 1-2 crater radii).

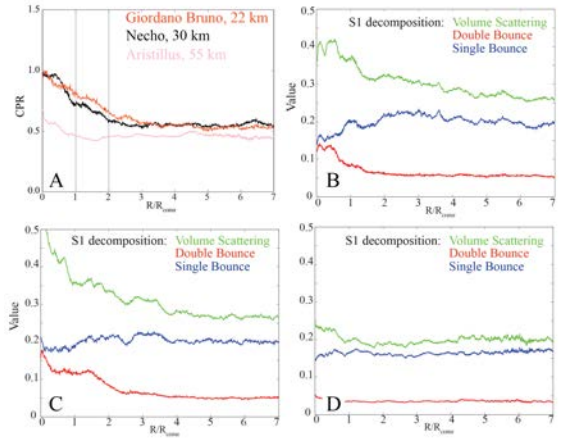

Fig. 3. A) CPR profiles for three craters as a function of crater radius outward from the crater rim; B) *m*-χ decomposition of S_1 for Necho crater (Highlands, 30 km); C) *m*-χ decomposition of S_1 for the crater Giordano Bruno (Highlands, 22 km); D) *m*-χ decomposition of S_1 for Aristillus crater (Mare, 55 km).

Profiles of the *m*-χ decomposition for crater ejecta blankets exhibits differences between terrains that are likely related to processes that effect CPR. However, there is variety among craters of a given terrain, when observed with this product, that potentially indicate the effects of additional processes. We have categorized *m*-χ decomposition profiles for the craters studied here into three types (Table 1). One end-member, Type 1, is characterized by high volume scattering component and approximately equal double and single bounce scattering near the crater, evolving to a consistent background signal at larger distances (Fig. 3B). Approximately 50% of studied craters fall into this category and it is largely dominated by highland craters. The other end-member, Type 3, is characterized by relatively constant values for all three scattering components (Fig. 3D). Type 2 is intermediate between the end-members (Fig. 3C).

Table 1. Classifications of craters based on *m*-χ profiles. Crater names in italics are in mare terrains.

	Characteristics	Craters
1	High volume scattering component. Approx. equal double and single bounce near crater	*Dionysius*, *Petavius B,* Furnerius A, Dufay B, Byrgius A, Proclus, Necho, Thales, Schomberger A, Anaxagoras
2	Intermediate profile shapes	*Bessarion, Gambart A, Euler, Kepler,* Dugan J, Klute W, Giordano Bruno
3	Approximately constant volume scattering, single and double bounce as a function of radius	*Harpalus E, Louville D, Harpalus, Aristillus,* Birkhoff Y, Guthnick, Bel'kovich K

Conclusions: The craters studied here demonstrate that CPR signatures differ between mare and highlands regions, and have (with few exceptions) logical progressions with crater size. For example, larger craters tend to have higher CPR near the crater rim than smaller craters within similar terrains. For the majority of highlands craters (and for select mare craters), the CPR profile is characterized by a "bench" of high CPR before evolving to lunar background values, likely representing areas of ejecta mixing with lunar regolith.

The *m*-χ story is less straightforward, however. Craters in both major terrain types, and across diameter ranges, fall into each of three categories. Possible variables that could affect the scattering characteristics include: crater age and degradation state, terrain type, local variations within terrains (e.g., layering), or crater diameter. Further study is necessary to fully understand the range of signatures that is observed.

In general, radar returns from the young craters observed here provide insight into the scattering properties of ejecta blankets, differentiation between ejecta properties in different lunar terrains, and possible identification of styles of ejecta deposition and mixing. These analyses improve our understanding of the primary weathering process on the moon, and how ejecta emplacement processes modify the lunar surface.

References: [1] Melosh, H. J. (1989), Oxford Univ. Press; [2] Campbell et al. (2010), *Icarus*, 208, 565-573; [3] Raney, R. K. et al. (2011), *Proc. of the IEEE*, 99, 808-823; [4] Patterson et al. (2013) *LPSC 44,* #2380; [5] Stokes (1852), Trans. of the Cambridge Phil. Soc. 9, 399; [6] Carter et al. (2012), JGR, 117, E00H09; [7] Raney, R.K. et al. (2012), *JGR,* 117, E00H21; [8] Moore et al. 1974, *Proc. 5th LPSC,* 71-100.